Mathematical modelling and virtual decomposition control of heavy-duty parallel−serial hydraulic manipulators

supplementary material, notes

Goran Petrović and Jouni Mattila

Tampere University: Tampereen yliopisto

October 10, 2021

Tampere, Finland

This supplementary file intends to provide more insight into the force calculation procedure proposed in the paper, using the real-world hydraulic manipulator model as an example.

Although the simulation file with all the required calculations is provided, this supplementary note will serve the purpose of emphasizing specific steps in the calculation process following the proposed notation and novel decomposition, intending to provide even more insight into kinematics and dynamics modelling.

In the provided simulation file, forces in linear hydraulic actuators are calculated in parallel using both Simscape Multibody™ and analytical results proposed in the paper. At the same time, values for generalized coordinates are directly commanded. The provided simulation file as-is fully proves the modelling concept.

Please note that in the attached simulation file, generalized coordinates change as sinusoids. This can be changed, but the first and second input signal derivatives should also be provided analytically or numerically.

CAD models of all hydraulic manipulator constituting parts are provided, allowing measurement of all lengths and angles of interest quickly and calculating mass properties of any rigid body of interest. These are all already determined in advance, and corresponding values are provided in the simulation initialization file.

Inertial properties of rigid bodies were directly written in the simulation to avoid direct calculation from a CAD file as an additional potential source of discrepancies.

The supplementary material at
`https://se.mathworks.com/matlabcentral/fileexchange/98464-hydraulic-manipulator-forces-modelling`
and/or `https://github.com/petrovicrgoran/ForcesModelling` contains the following:

a) textual files:
   - *SupplementaryNotesGP.pdf* - this file

b) MATLAB/Simulink files:
   - *InitializeSimulationGP.m* - simulation initialization file,
   - *SimForcesGP2020a.slx* - Simulink simulation file for MATLAB versions 2020a and newer,
   - *SimForcesGP2017a.slx* - Simulink simulation file for MATLAB versions 2017a and newer,

c) CAD models:
   - *01_BaseGP.STEP*,
   - *02_LiftLinkGP.STEP*,
   - *03_LiftCylGP.STEP*,
   - *04_LiftPistGP.STEP*,
   - *05_TiltCylGP.STEP*,
   - *06_TiltPistGP.STEP*,
   - *07_TiltLinkGP.STEP*,
   - *08_ExtCyl1GP.STEP*,
   - *09_ExtPist1GP.STEP*,
   - *10_ObjectGP.STEP*.

All the credit for CAD models goes to Dr Janne Koivumäki, who created them from scratch during his work on MSc and PhD theses at IHA laboratory, Tampere University.

Friendly suggestions and valuable tips from Pauli Mustalahti and Lionel Hulttinen are kindly acknowledged.

For all the questions and feedback, please contact goran.petrovic@tuni.fi.

Authors

Goran Petrović
`https://www.researchgate.net/profile/Goran-Petrovic-9`

Dr Jouni Mattila
`https://www.researchgate.net/profile/Jouni-Mattila`

Hydraulic manipulator

Figure 1 shows different constituting parts of the manipulator considered, with every part labeled using numbers from 1 to 10. For each part, a CAD model is provided. Each file is named in accordance with the corresponding label in Fig. 1 and file names are: *01_BaseGP.STEP*, *02_LiftLinkGP.STEP*, *03_LiftCylGP.STEP*, *04_LiftPistGP.STEP*, *05_TiltCylGP.STEP*, *06_TiltPistGP.STEP*, *07_TiltLinkGP.STEP*, *08_ExtCyl1GP.STEP*, *09_ExtPist1GP.STEP*, *10_ObjectGP.STEP*, respectively.

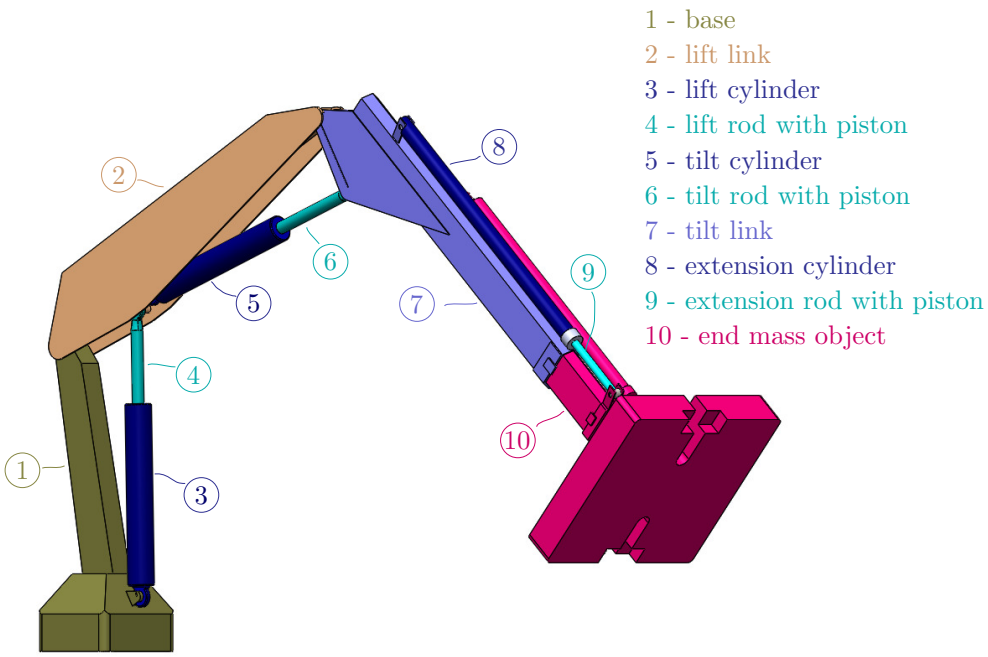

Figure 1: Manipulator assembly and its constituting parts.

Figure 2 shows the manipulator, conceptually divided into structures in series, as proposed in the paper. The considered manipulator can be divided into two generic manipulator structures. Structure 1 contains only revolute segment, and structure 2 contains both revolute segment with passive revolute joint actuated by a linear hydraulic actuator and prismatic segment with prismatic joint, also actuated by a linear hydraulic actuator.

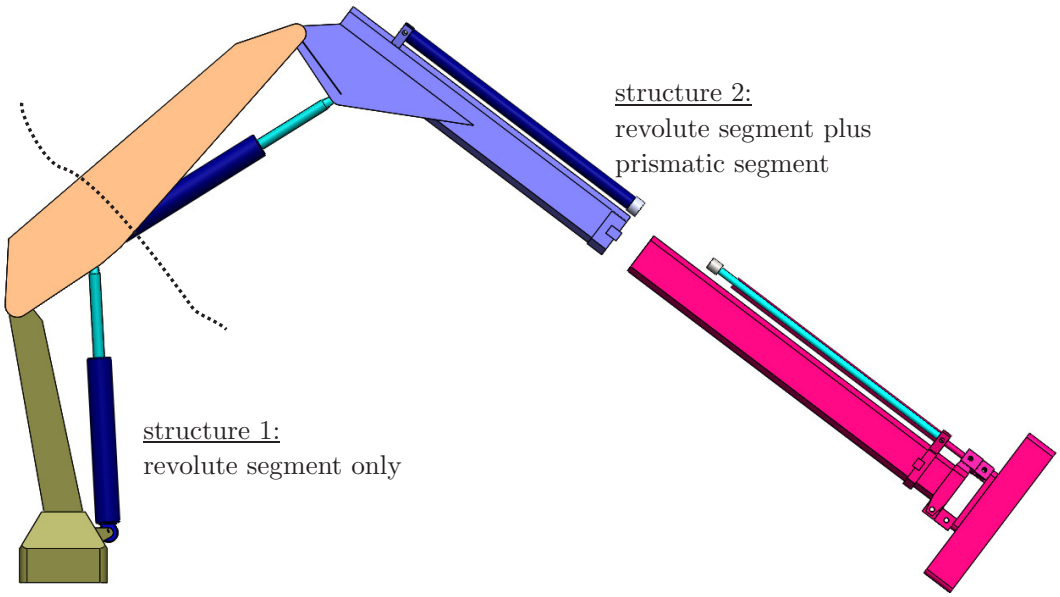

Figure 2: Manipulator assembly conceptually divided into structures.

Figure 3 shows the chosen set of generalized coordinates used both in the following analytic expressions and in the Simscape to command the manipulator motion.

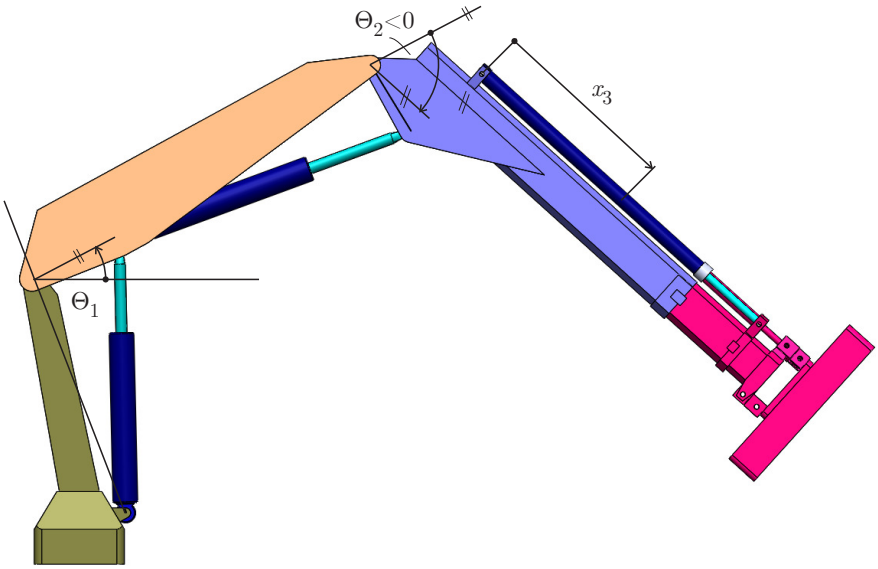

Figure 3: Manipulator assembly with chosen generalized coordinates.

Manipulator structure 1

Manipulator structure 1 contains only the revolute segment from Fig. 4 – 5, where the notation is in accordance with the one proposed in the paper. Figure 5 shows the revolute segment 1 with required frames for addressing the kinematics and dynamics. Since there is no prismatic segment, and a revolute segment follows, frames $\{\mathbf{E_{11}}\}$ and $\{\mathbf{B_{c2}}\}$ are coincident, $\{\mathbf{E_{11}}\} = \{\mathbf{B_{c2}}\}$, and frame $\{\mathbf{P_{21}}\}$ does not exist in the structure 1.

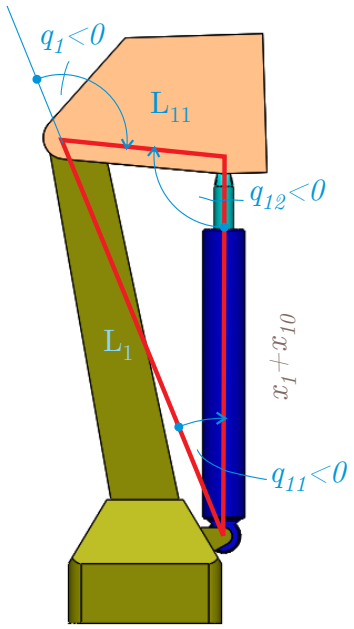

Figure 4: Manipulator structure 1 with its corresponding lengths and angles.

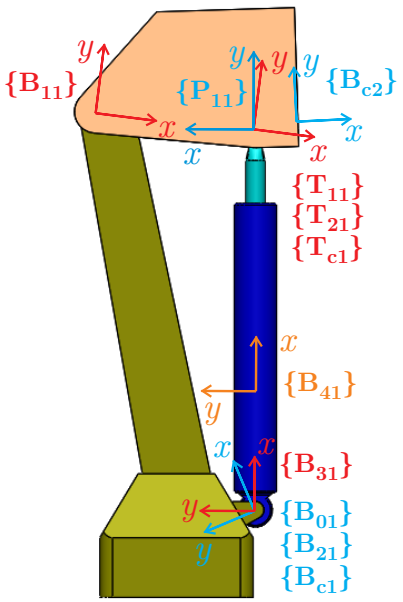

Figure 5: Manipulator structure 1 with its corresponding frames.

Revolute segment in the manipulator structure 1

It is assumed that linear/angular velocity vector ${}^{\mathbf{B_{c1}}}\boldsymbol{V}$ is known from previous calculations. Assuming fixed base, this vector is zero vector, ${}^{\mathbf{B_{c1}}}\boldsymbol{V} = \mathbf{0}$. All the fixed distances and angles are assumed to be accurately known from CAD models and thus all the constant position vectors, as all the constant rotation matrices.

In addition, all inertia tensors and masses required for dynamics calculations can be obtained from CAD software. Exact numerical values can be found in the attached MATLAB initialization file.

Loop-closure functions

Geometric relations in the closed kinematic loop are calculated at every time instant as:

$$x_1 = \sqrt{L_1^2 + L_{11}^2 + 2\,L_1\,L_{11}\,\cos q_1} - x_{10}, \tag{1}$$

$$q_{11} = -\arccos\left(\frac{L_{11}^2 - (x_1 + x_{10})^2 - L_1^2}{-2\,(x_1 + x_{10})\,L_1}\right), \tag{2}$$

and

$$q_{12} = -\arccos\left(\frac{L_1^2 - (x_1 + x_{10})^2 - L_{11}^2}{-2\,(x_1 + x_{10})\,L_{11}}\right), \tag{3}$$

where:

$$q_1 = -2.0736 - \Theta_1, \tag{4}$$

with Θ_1 given in radians.

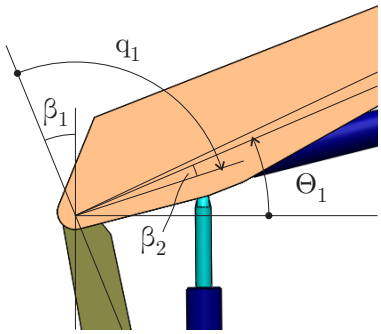

Figure 6: Relating angles Θ_1 and q_1.

The rationale behind Eq. (4) comes from Fig. 6, with values for β_1 and β_2 found from CAD software as shown in Fig. 7 and defined in the initialization file.

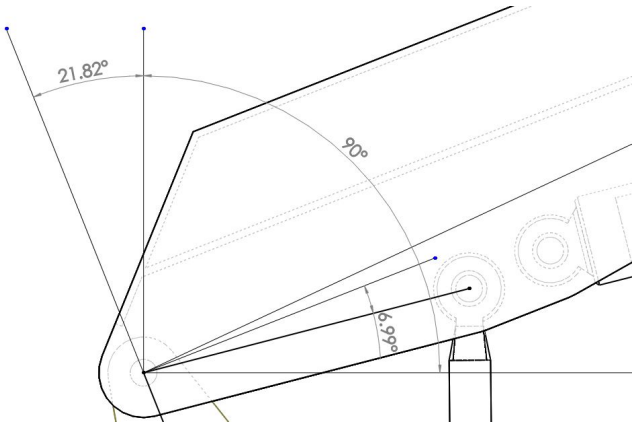

Figure 7: Relating angles Θ_1 and q_1 using CAD software.

Important closed-loop velocities can be calculated here as:

$$\dot{x}_1 = -\frac{L_1\, L_{11}\, \sin q_1}{x_1 + x_{10}}\, \dot{q}_1, \tag{5}$$

$$\dot{q}_{11} = -\frac{(x_1 + x_{10}) - L_1\, \cos q_{11}}{(x_1 + x_{10})\, L_1\, \sin q_{11}}\, \dot{x}_1, \tag{6}$$

$$\dot{q}_{12} = -\frac{(x_1 + x_{10}) - L_{11}\, \cos q_{12}}{(x_1 + x_{10})\, L_{11}\, \sin q_{12}}\, \dot{x}_1. \tag{7}$$

Manipulator base

The manipulator base is shown in more detail in Figure 8 with all the relevant attached frames. Many appropriate steps required in the modelling process will be emphasised in the manipulator base case since it is the first to be considered. The reason for this is to avoid unnecessary repeatability, which would not introduce much new information. The same approach, shown in more detail once, can be then later applied in the case of every manipulator part.

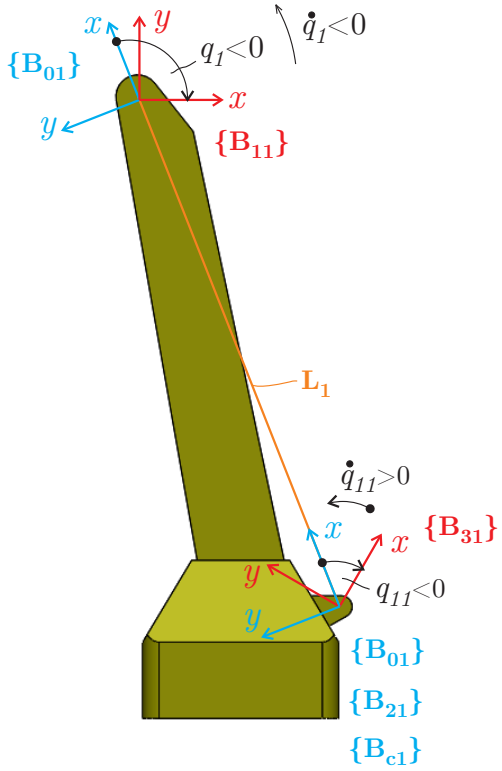

Figure 8: Manipulator base with attached frames.

Frames $\{\mathbf{B_{01}}\}$, $\{\mathbf{B_{21}}\}$ and $\{\mathbf{B_{c1}}\}$ are coincident at the q_{11}-joint, as stated in the paper. It is only for the better illustration purpose that the frame $\{\mathbf{B_{01}}\}$ is shown next to the $\{\mathbf{B_{11}}\}$, frame at the q_1-joint.

Constant position vectors ${}^{\mathbf{B_{c1}}}\boldsymbol{r}_{\mathbf{B_{c1}B_{11}}} = \begin{pmatrix} L_1 \\ 0 \\ 0 \end{pmatrix}$, ${}^{\mathbf{B_{c1}}}\boldsymbol{r}_{\mathbf{B_{c1}B_{31}}} = \begin{pmatrix} 0 \\ 0 \\ 0 \end{pmatrix}$, in combination with time-varying rotation matrices:

$${}^{\mathbf{B_{c1}}}\mathbf{R}_{\mathbf{B_{11}}} = \begin{pmatrix} \cos q_1 & -\sin q_1 & 0 \\ \sin q_1 & \cos q_1 & 0 \\ 0 & 0 & 1 \end{pmatrix} \tag{8}$$

and

$${}^{\mathbf{B_{01}}}\mathbf{R}_{\mathbf{B_{31}}} = {}^{\mathbf{B_{21}}}\mathbf{R}_{\mathbf{B_{31}}} = {}^{\mathbf{B_{c1}}}\mathbf{R}_{\mathbf{B_{31}}} = \begin{pmatrix} \cos q_{11} & -\sin q_{11} & 0 \\ \sin q_{11} & \cos q_{11} & 0 \\ 0 & 0 & 1 \end{pmatrix}, \tag{9}$$

can be used to form time-varying transformation matrices ${}^{\mathbf{B_{c1}}}\mathbf{U}_{\mathbf{B_{11}}}$ and ${}^{\mathbf{B_{c1}}}\mathbf{U}_{\mathbf{B_{31}}}$ as:

$$ {}^{\mathbf{B_{c1}}}\mathbf{U}_{\mathbf{B_{11}}} = \begin{pmatrix} \cos q_1 & -\sin q_1 & 0 & 0 & 0 & 0 \\ \sin q_1 & \cos q_1 & 0 & 0 & 0 & 0 \\ 0 & 0 & 1 & 0 & 0 & 0 \\ 0 & 0 & 0 & \cos q_1 & -\sin q_1 & 0 \\ 0 & 0 & -L_1 & \sin q_1 & \cos q_1 & 0 \\ L_1 \sin q_1 & L_1 \cos q_1 & 0 & 0 & 0 & 1 \end{pmatrix}, \tag{10} $$

and

$$ {}^{\mathbf{B_{c1}}}\mathbf{U}_{\mathbf{B_{31}}} = \begin{pmatrix} \cos q_{11} & -\sin q_{11} & 0 & 0 & 0 & 0 \\ \sin q_{11} & \cos q_{11} & 0 & 0 & 0 & 0 \\ 0 & 0 & 1 & 0 & 0 & 0 \\ 0 & 0 & 0 & \cos q_{11} & -\sin q_{11} & 0 \\ 0 & 0 & 0 & \sin q_{11} & \cos q_{11} & 0 \\ 0 & 0 & 0 & 0 & 0 & 1 \end{pmatrix}, \tag{11} $$

per known relation:

$$ {}^{\mathbf{A}}\mathbf{U}_{\mathbf{B}} = \begin{pmatrix} {}^{\mathbf{A}}\mathbf{R}_{\mathbf{B}} & \mathbf{O}_{3\times 3} \\ \left({}^{\mathbf{A}}\boldsymbol{r}_{\mathbf{AB}}\times\right){}^{\mathbf{A}}\mathbf{R}_{\mathbf{B}} & {}^{\mathbf{A}}\mathbf{R}_{\mathbf{B}} \end{pmatrix}. \tag{12} $$

Analytic expressions for all the remaining rotation ${}^{\mathbf{A}}\mathbf{R}_{\mathbf{B}}$ and force/velocity transformation matrices ${}^{\mathbf{A}}\mathbf{U}_{\mathbf{B}}$ will not be written explicitly in the following text. The reason is unnecessary repeatability, while the way they are all separately formed can be seen in the simulation file.

Matrices $\mathbf{M}_{\mathbf{A}}$, $\mathbf{C}_{\mathbf{A}}\left({}^{\mathbf{A}}\boldsymbol{\omega}\right)$ and vector $\mathbf{G}_{\mathbf{A}}$ are formed per known expressions:

$$ \mathbf{M}_{\mathbf{A}} \overset{\text{def}}{=} \begin{pmatrix} m\,\mathrm{I}_{3\times 3} & -m\left({}^{A}\mathbf{r}_{AB}\times\right) \\ m\left({}^{A}\mathbf{r}_{AB}\times\right) & \left[{}^{A}\mathbf{I}\right] - m\left({}^{A}\mathbf{r}_{AB}\times\right)^2 \end{pmatrix}, \tag{13} $$

$$ \mathbf{C}_{\mathbf{A}}\left({}^{A}\boldsymbol{\omega}\right) \overset{\text{def}}{=} \begin{pmatrix} m\left({}^{A}\boldsymbol{\omega}\times\right) & -m\left({}^{A}\boldsymbol{\omega}\times\right)\left({}^{A}\mathbf{r}_{AB}\times\right) \\ m\left({}^{A}\mathbf{r}_{AB}\times\right)\left({}^{A}\boldsymbol{\omega}\times\right) & -m\left({}^{A}\mathbf{r}_{AB}\times\right)\left({}^{A}\boldsymbol{\omega}\times\right)\left({}^{A}\vec{\mathbf{r}}_{AB}\times\right) + \left[{}^{A}\mathbf{I}\right]\left({}^{A}\boldsymbol{\omega}\times\right) + \left({}^{A}\boldsymbol{\omega}\times\right)\left[{}^{A}\mathbf{I}\right] \end{pmatrix}, \tag{14} $$

and

$$ \mathbf{G}_{\mathbf{A}} = \begin{pmatrix} m\,{}^{A}\mathbf{R}_{W}\,{}^{W}\mathbf{g} \\ m\left({}^{A}\mathbf{r}_{AB}\times\right){}^{A}\mathbf{R}_{W}\,{}^{W}\mathbf{g} \end{pmatrix}, \tag{15} $$

with A denoting any frame $\{\mathbf{A}\}$ attached to the rigid body, while the origin of frame $\{\mathbf{B}\}$ coincides with the body's center of mass. Finally, W denotes the fixed world frame $\{\mathbf{W}\}$ with a clearly defined origin.

An analytic expression for every separate case will not be shown because of the expression complexity, but the way they all are formed can be seen in the simulation file.

Inertia tensor $\left[{}^{A}\mathbf{I}\right]$ contains moments of inertia about the centre of mass, expressed in frame $\{\mathbf{A}\}$. For any general frame $\{\mathbf{A}\}$, the tensor can be found from the CAD software with prior defining of the frame itself.

For example, frame $\{\mathbf{B_{c1}}\}$ is introduced in SolidWorks™ as in Fig. 9 for the manipulator base.

Figure 10 shows manipulator base moments of inertia about its centre of mass and expressed in the $\{\mathbf{B_{c1}}\}$ frame. It is worth noting that off-diagonal terms are defined per SolidWorks™ convention without a minus sign.

Inertial data in the simulation can be entered manually or automatically inferred based on the provided mass or density of the solid part considered. In the provided simulation file, these are entered manually. It is worth noting that entered values must be provided in the part's reference frame. Figure 11 shows values obtained for the manipulator base, used to initialize inertial data in the simulation, per Fig. 12. The correspondence between these two is self-explanatory.

Another thing to note is that the gravity vector in equations, having the form proposed in the paper, participates on the opposite side of the forcing terms, and thus, the care of its sign should be taken following the defined world frame. Here, although the gravity vector is assumed to have a negative projection on the world frame y-axis, the vector ${}^{W}\mathbf{g}$ used in calculations is defined as:

$$ {}^{W}\mathbf{g} = \begin{pmatrix} 0 \\ 9.8066 \\ 0 \end{pmatrix}. \tag{16} $$

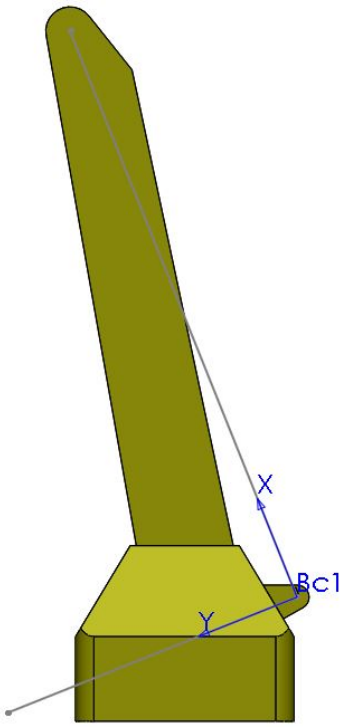

Figure 9: Manipulator base with the $\{\mathbf{B_{c1}}\}$ frame introduced in the analysis.

Report coordinate values relative to: Bc1

Mass = 307.29601379 kilograms

Volume = 0.04209534 cubic meters

Surface area = 0.98157989 square meters

Center of mass: (meters)
X = 0.14178771
Y = 0.16555780
Z = 0.00000000

Principal axes of inertia and principal moments of inertia: (kilograms * square meters)
Taken at the center of mass.

Ix = (0.97499457, -0.22222870, 0.00000000)	Px = 4.64405122
Iy = (-0.00004850, -0.00021522, -0.99999998)	Py = 29.78955949
Iz = (0.22222869, 0.97499454, -0.00022062)	Pz = 29.91781588

Moments of inertia: (kilograms * square meters)
Taken at the center of mass and aligned with the output coordinate system.

Lxx = 5.89221108	Lxy = -5.47611136	Lxz = 0.00001963
Lyx = -5.47611136	Lyy = 28.66965601	Lyz = 0.00002455
Lzx = 0.00001963	Lzy = 0.00002455	Lzz = 29.78955950

Moments of inertia: (kilograms * square meters)
Taken at the output coordinate system.

Ixx = 14.31500622	Ixy = 1.73737430	Ixz = -0.00000113
Iyx = 1.73737430	Iyy = 34.84745975	Iyz = 0.00000031
Izx = -0.00000113	Izy = 0.00000031	Izz = 44.39015837

Figure 10: Manipulator base moments of inertia about the c.o.m expressed in the $\{\mathbf{B_{c1}}\}$ frame.

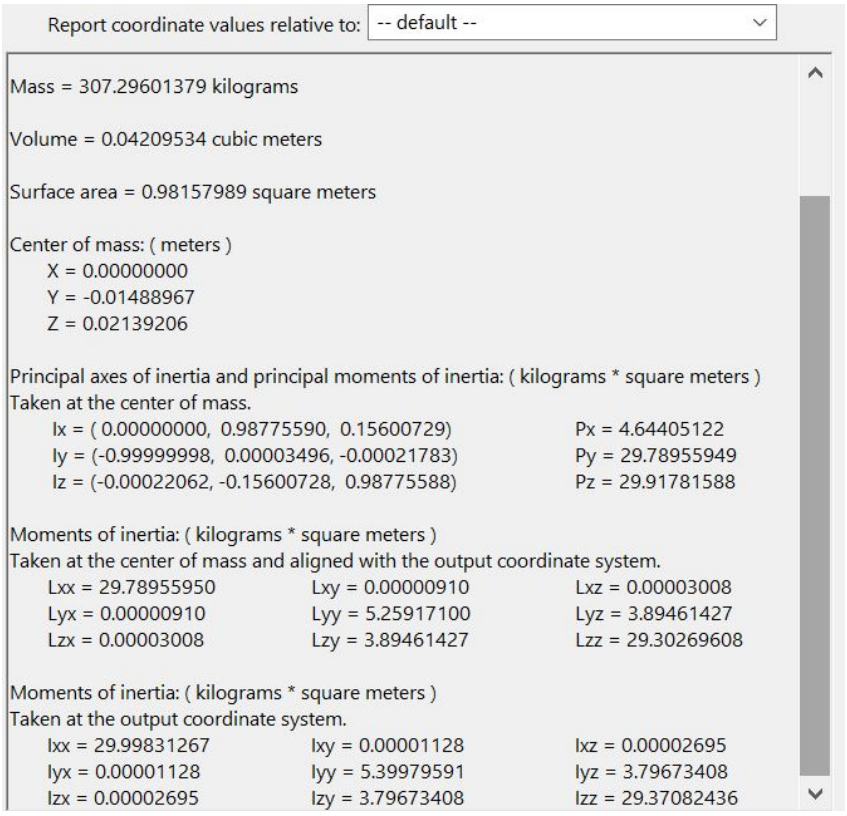

Figure 11: Manipulator base moments of inertia about the c.o.m expressed in the CAD model reference frame.

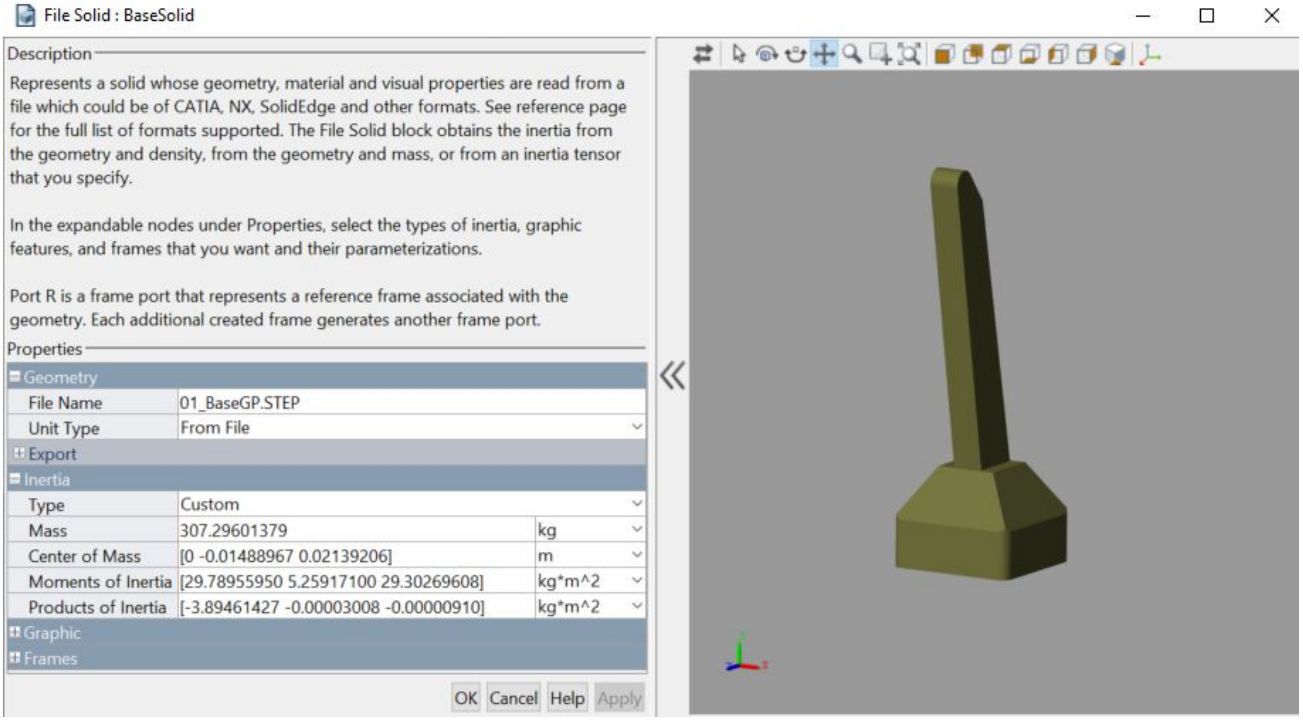

Figure 12: Entering manipulator base inertial data in the simulation environment.

The total forces/moments acting on the base can be now calculated as:

$$\mathbf{M}_{\mathbf{B_{c1}}} \frac{\mathrm{d}}{\mathrm{d}t} \left({}^{\mathbf{B_{c1}}}\boldsymbol{V} \right) + \mathbf{C}_{\mathbf{B_{c1}}} \left({}^{\mathbf{B_{c1}}}\boldsymbol{\omega} \right) {}^{\mathbf{B_{c1}}}\boldsymbol{V} + \mathbf{G}_{\mathbf{B_{c1}}} = {}^{\mathbf{B_{c1}}}\boldsymbol{F}^{*}, \tag{17}$$

using data from Fig. 10.

Lift cylinder and lift rod with piston

In the case of the lift cylinder and lift rod with piston, it can be noted that the position vector ${}^{\mathbf{B_{31}}}\boldsymbol{r}_{\mathbf{B_{31}B_{41}}}$ is not fixed, but is a function of the piston displacement x_1.

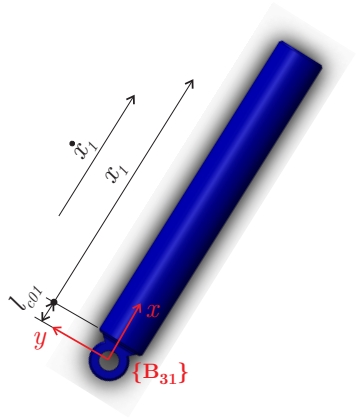

Figure 13: Lift cylinder.

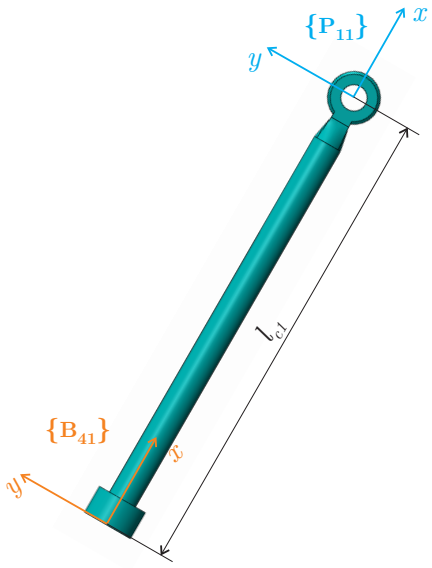

Figure 14: Lift rod with piston.

Velocities requiring calculation are:

$$ {}^{\mathbf{B_{31}}}\boldsymbol{V} = \mathbf{z}_\tau \, \dot{q}_{11} + {}^{\mathbf{B_{c1}}}\mathbf{U}^T_{\mathbf{B_{31}}} \, {}^{\mathbf{B_{c1}}}\boldsymbol{V}, \tag{18} $$

$$ {}^{\mathbf{B_{41}}}\boldsymbol{V} = \mathbf{x}_f \, \dot{x}_1 + {}^{\mathbf{B_{31}}}\mathbf{U}^T_{\mathbf{B_{41}}} \, {}^{\mathbf{B_{31}}}\boldsymbol{V}, \tag{19} $$

and

$$ {}^{\mathbf{T_{21}}}\boldsymbol{V} = \mathbf{z}_\tau \, \dot{q}_{12} + {}^{\mathbf{B_{41}}}\mathbf{U}^T_{\mathbf{T_{21}}} \, {}^{\mathbf{B_{41}}}\boldsymbol{V}. \tag{20} $$

Finally, linear/angular velocities measured and expressed in the frame $\{\mathbf{B_{c2}}\}$ can be calculated as:

$$ {}^{\mathbf{B_{c2}}}\boldsymbol{V} = {}^{\mathbf{T_{21}}}\mathbf{U}^T_{\mathbf{B_{c2}}} \, {}^{\mathbf{T_{21}}}\boldsymbol{V}. \tag{21} $$

Total forces/moments requiring calculation are:

$$ \mathbf{M}_{\mathbf{B_{31}}} \frac{\mathrm{d}}{\mathrm{d}t} \left({}^{\mathbf{B_{31}}}\boldsymbol{V} \right) + \mathbf{C}_{\mathbf{B_{31}}} \left({}^{\mathbf{B_{31}}}\boldsymbol{\omega} \right) {}^{\mathbf{B_{31}}}\boldsymbol{V} + \mathbf{G}_{\mathbf{B_{31}}} = {}^{\mathbf{B_{31}}}\boldsymbol{F}^*. \tag{22} $$

and

$$ \mathbf{M}_{\mathbf{B_{41}}} \frac{\mathrm{d}}{\mathrm{d}t} \left({}^{\mathbf{B_{41}}}\boldsymbol{V} \right) + \mathbf{C}_{\mathbf{B_{41}}} \left({}^{\mathbf{B_{41}}}\boldsymbol{\omega} \right) {}^{\mathbf{B_{41}}}\boldsymbol{V} + \mathbf{G}_{\mathbf{B_{41}}} = {}^{\mathbf{B_{41}}}\boldsymbol{F}^*. \tag{23} $$

.

Lift link

The lift link partially belongs to the manipulator structure 1 and partially to the manipulator structure 2. This is why it is virtually cut and why two total force equations must be formed.

The velocity term to be calculated is:

$$ {}^{\mathbf{B_{11}}}\mathbf{V} = \mathbf{z}_\tau \, \dot{q}_1 + {}^{\mathbf{B_{c1}}}\mathbf{U}^T_{\mathbf{B_{11}}} \, {}^{\mathbf{B_{c1}}}\boldsymbol{V}, \tag{24} $$

and the two total force/moment vectors are:

$$ \mathbf{M}_{\mathbf{B_{11}}} \frac{\mathrm{d}}{\mathrm{d}t} \left({}^{\mathbf{B_{11}}}\boldsymbol{V} \right) + \mathbf{C}_{\mathbf{B_{11}}} \left({}^{\mathbf{B_{11}}}\boldsymbol{\omega} \right) {}^{\mathbf{B_{11}}}\boldsymbol{V} + \mathbf{G}_{\mathbf{B_{11}}} = {}^{\mathbf{B_{11}}}\boldsymbol{F}^*. \tag{25} $$

$$ \mathbf{M}_{\mathbf{B_{c2}}} \frac{\mathrm{d}}{\mathrm{d}t} \left({}^{\mathbf{B_{c2}}}\boldsymbol{V} \right) + \mathbf{C}_{\mathbf{B_{c2}}} \left({}^{\mathbf{B_{c2}}}\boldsymbol{\omega} \right) {}^{\mathbf{B_{c2}}}\boldsymbol{V} + \mathbf{G}_{\mathbf{B_{c2}}} = {}^{\mathbf{B_{c2}}}\boldsymbol{F}^*. \tag{26} $$

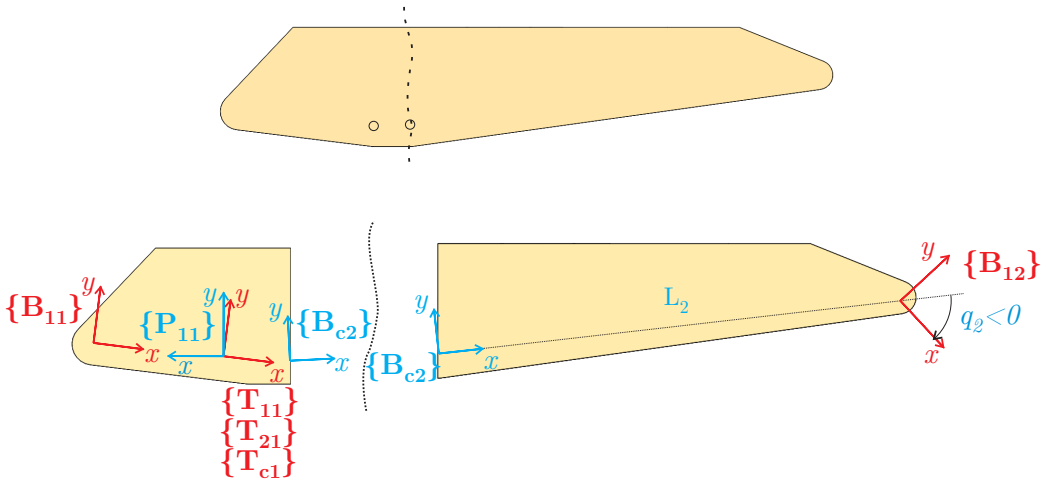

Figure 15: Lift link before and after virtual cutting

Manipulator structure 2

Manipulator structure 2 is shown in Figure 16, with relevant frames, angles and lenghts, where because of the prismatic segment existence $\{\mathbf{E_{12}}\} = \{\mathbf{P_{22}}\}$, and because of the end-effector presence $\{\mathbf{E_{22}}\} = \{\mathbf{D_{22}}\}$.

Geometric relations in the closed kinematic loop are calculated at every time instant as:

$$x_2 = \sqrt{L_2^2 + L_{21}^2 + 2\,L_2\,L_{21}\,\cos q_2} - x_{20}, \tag{27}$$

$$q_{21} = -\arccos\left(\frac{L_{21}^2 - (x_2 + x_{20})^2 - L_2^2}{-2\,(x_2 + x_{20})\,L_2}\right), \tag{28}$$

and

$$q_{22} = -\arccos\left(\frac{L_2^2 - (x_2 + x_{20})^2 - L_{21}^2}{-2\,(x_2 + x_{20})\,L_{21}}\right), \tag{29}$$

with:

$$q_2 = \Theta_2 - 0.4116, \tag{30}$$

with Θ_2 in radians, as illustrated in Fig. 17.

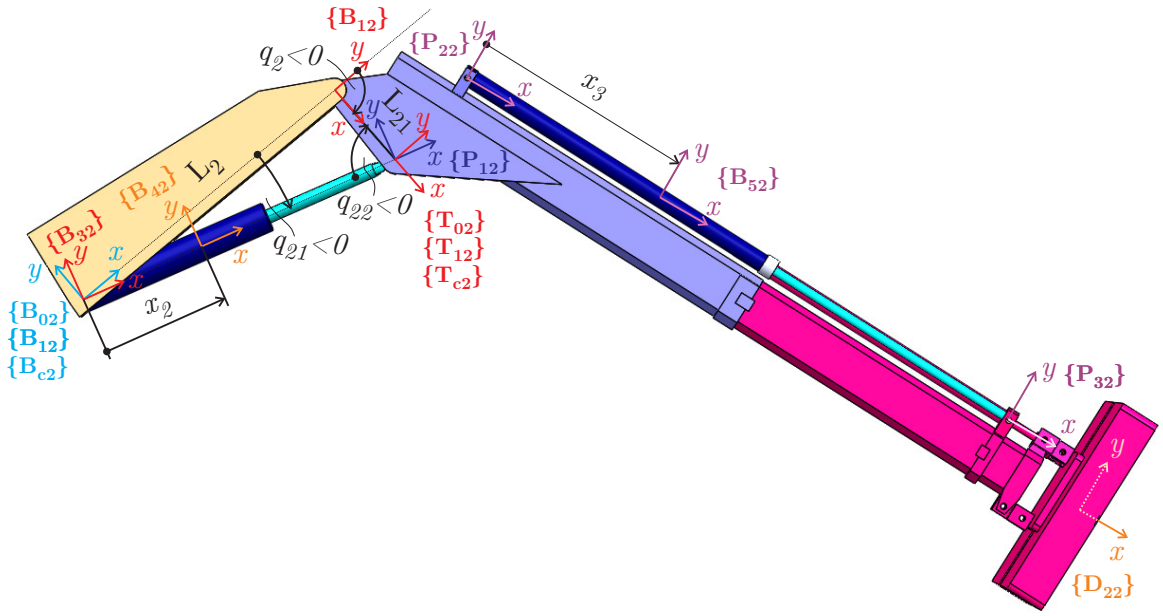

Figure 16: Manipulator structure 2.

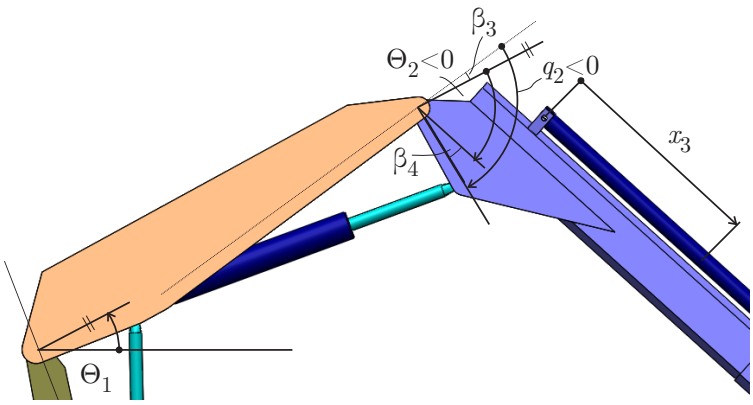

Figure 17: Relating angles Θ_2 and q_2.

Same as in the case of manipulator structure 1, important time rates of change can be calculated as:

$$\dot{x}_2 = -\frac{L_2\, L_{21}\, \sin q_2}{x_2 + x_{20}}\, \dot{q}_2, \tag{31}$$

$$\dot{q}_{21} = -\frac{(x_2 + x_{20}) - L_2\, \cos q_{21}}{(x_2 + x_{20})\, L_2\, \sin q_{21}}\, \dot{x}_2, \tag{32}$$

$$\dot{q}_{22} = -\frac{(x_2 + x_{20}) - L_{21}\, \cos q_{22}}{(x_2 + x_{20})\, L_{21}\, \sin q_{22}}\, \dot{x}_2. \tag{33}$$

Tilt cylinder and lift rod with piston

The tilt cylinder and rod with piston are the same as the lift counterparts.

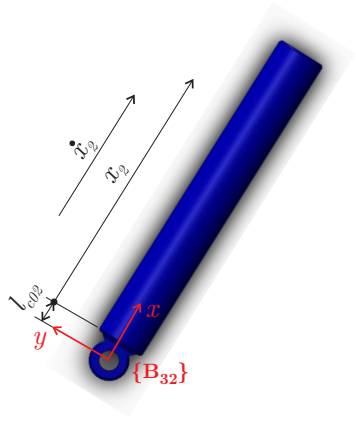

Figure 18: Tilt cylinder.

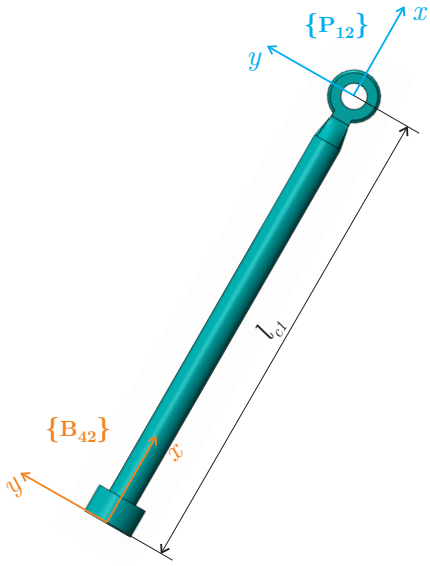

Figure 19: Tilt rod with piston.

Velocities to be calculated and used in the later calculations are:

$$^{\mathbf{B_{32}}}\boldsymbol{V} = \mathbf{z}_\tau\, \dot{q}_{21} + {}^{\mathbf{B_{c2}}}\mathbf{U}^T_{\mathbf{B_{32}}}\, {}^{\mathbf{B_{c2}}}\boldsymbol{V}, \tag{34}$$

and

$$^{\mathbf{B_{42}}}\boldsymbol{V} = \mathbf{x}_f\, \dot{x}_2 + {}^{\mathbf{B_{32}}}\mathbf{U}^T_{\mathbf{B_{42}}}\, {}^{\mathbf{B_{32}}}\boldsymbol{V}. \tag{35}$$

The total force/moment vectors in this case are:

$$\mathbf{M}_{\mathbf{B_{32}}} \frac{\mathrm{d}}{\mathrm{d}t}\left({}^{\mathbf{B_{32}}}\boldsymbol{V}\right) + \mathbf{C}_{\mathbf{B_{32}}}\left({}^{\mathbf{B_{32}}}\boldsymbol{\omega}\right) {}^{\mathbf{B_{32}}}\boldsymbol{V} + \mathbf{G}_{\mathbf{B_{32}}} = {}^{\mathbf{B_{32}}}\boldsymbol{F}^*, \tag{36}$$

and

$$\mathbf{M}_{\mathbf{B_{42}}} \frac{\mathrm{d}}{\mathrm{d}t}\left({}^{\mathbf{B_{42}}}\boldsymbol{V}\right) + \mathbf{C}_{\mathbf{B_{42}}}\left({}^{\mathbf{B_{42}}}\boldsymbol{\omega}\right) {}^{\mathbf{B_{42}}}\boldsymbol{V} + \mathbf{G}_{\mathbf{B_{42}}} = {}^{\mathbf{B_{42}}}\boldsymbol{F}^*. \tag{37}$$

Tilt link

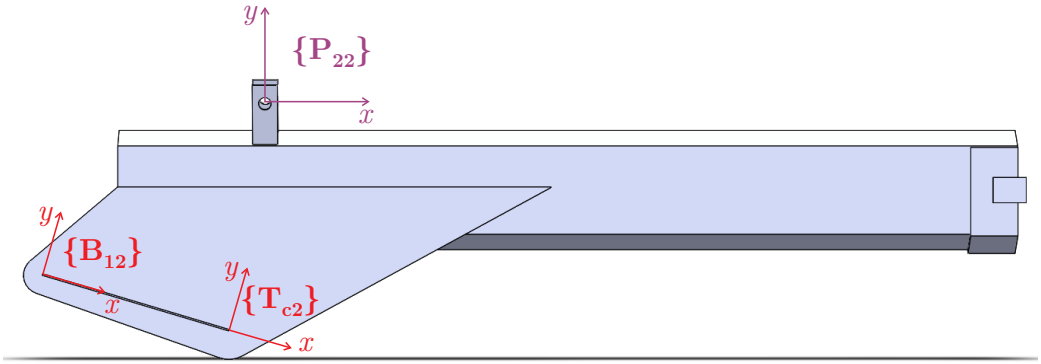

Figure 20: Tilt link.

The tilt link, shown in Fig. 20, does not have to be virtually cut in this setup, following the approach presented in the paper. It is only required to calculate velocity vectors:

$$ {}^{\mathbf{B_{12}}}\mathbf{V} = \mathbf{z}_\tau \, \dot{q}_2 + {}^{\mathbf{B_{c2}}}\mathbf{U}^T_{\mathbf{B_{12}}} \, {}^{\mathbf{B_{c2}}}\boldsymbol{V}, \tag{38} $$

and

$$ {}^{\mathbf{T_{c2}}}\boldsymbol{V} = \mathbf{z}_\tau \, \dot{q}_{22} + {}^{\mathbf{B_{42}}}\mathbf{U}^T_{\mathbf{T_{c2}}} \, {}^{\mathbf{B_{42}}}\boldsymbol{V}, \tag{39} $$

along with the total force/moment vector:

$$ \mathbf{M}_{\mathbf{B_{12}}} \frac{\mathrm{d}}{\mathrm{d}t} \left({}^{\mathbf{B_{12}}}\boldsymbol{V} \right) + \mathbf{C}_{\mathbf{B_{12}}} \left({}^{\mathbf{B_{12}}}\boldsymbol{\omega} \right) {}^{\mathbf{B_{12}}}\boldsymbol{V} + \mathbf{G}_{\mathbf{B_{12}}} = {}^{\mathbf{B_{12}}}\boldsymbol{F}^*. \tag{40} $$

Prismatic segment's cylinder and rod with piston

Figures 21 − 22 show cylinder and rod with piston in the prismatic joint.

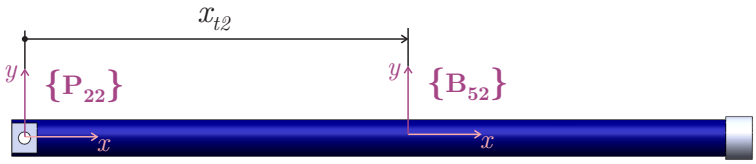

Figure 21: Prismatic joint cylinder.

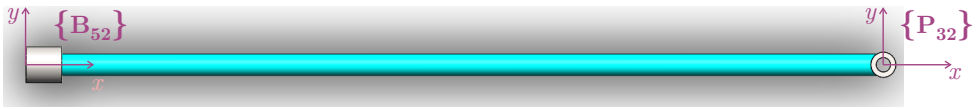

Figure 22: Prismatic joint rod with piston.

Velocities to be calculated are:

$$ {}^{\mathbf{P_{22}}}\mathbf{V} = {}^{\mathbf{T_{c2}}}\mathbf{U}^T_{\mathbf{P_{22}}} \, {}^{\mathbf{T_{c2}}}\boldsymbol{V}, \tag{41} $$

and:

$$ {}^{\mathbf{B_{52}}}\boldsymbol{V} = \mathbf{x}_f \, \dot{x}_{t2} + {}^{\mathbf{P_{22}}}\mathbf{U}^T_{\mathbf{B_{52}}} \, {}^{\mathbf{P_{22}}}\boldsymbol{V}, \tag{42} $$

with the total forces/moments to be calculated:

$$ \mathbf{M}_{\mathbf{P_{22}}} \frac{\mathrm{d}}{\mathrm{d}t} \left({}^{\mathbf{P_{22}}}\boldsymbol{V} \right) + \mathbf{C}_{\mathbf{P_{22}}} \left({}^{\mathbf{P_{22}}}\boldsymbol{\omega} \right) {}^{\mathbf{P_{22}}}\boldsymbol{V} + \mathbf{G}_{\mathbf{P_{22}}} = {}^{\mathbf{P_{22}}}\boldsymbol{F}^*, \tag{43} $$

and

$$ \mathbf{M}_{\mathbf{B_{52}}} \frac{\mathrm{d}}{\mathrm{d}t} \left({}^{\mathbf{B_{52}}}\boldsymbol{V} \right) + \mathbf{C}_{\mathbf{B_{52}}} \left({}^{\mathbf{B_{52}}}\boldsymbol{\omega} \right) {}^{\mathbf{B_{52}}}\boldsymbol{V} + \mathbf{G}_{\mathbf{B_{52}}} = {}^{\mathbf{B_{52}}}\boldsymbol{F}^*. \tag{44} $$

End mass object

Mass object, located at the end of the prismatic segment, containing the end-effector is shown in Fig. 23.

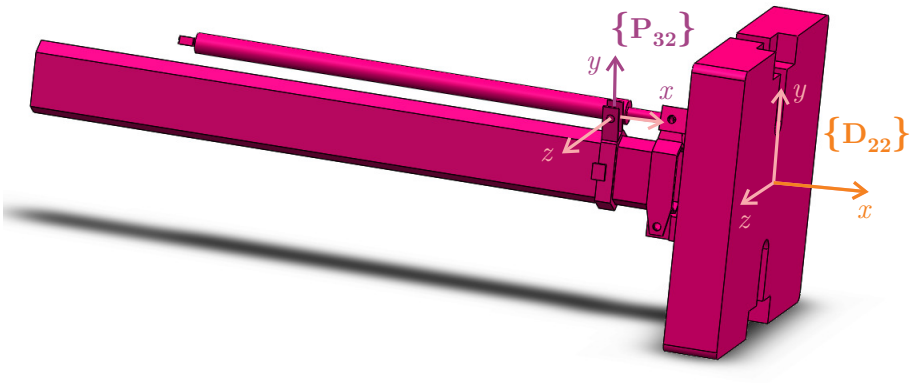

Figure 23: End mass object.

Final velocities to be calculated are:

$$ {}^{\mathbf{P_{32}}}\mathbf{V} = {}^{\mathbf{B_{52}}}\mathbf{U}^{T}_{\mathbf{P_{32}}}\, {}^{\mathbf{B_{52}}}\boldsymbol{V}. \tag{45} $$

Moreover, the total forces/moments are:

$$ \mathbf{M}_{\mathbf{P_{32}}} \frac{\mathrm{d}}{\mathrm{d}t}\left({}^{\mathbf{P_{32}}}\boldsymbol{V}\right) + \mathbf{C}_{\mathbf{P_{32}}}\left({}^{\mathbf{P_{32}}}\boldsymbol{\omega}\right) {}^{\mathbf{P_{32}}}\boldsymbol{V} + \mathbf{G}_{\mathbf{P_{32}}} = {}^{\mathbf{P_{32}}}\boldsymbol{F}^{*}. \tag{46} $$

Determination of actuator forces

Assuming that the force acting on the end-effector ${}^{\mathbf{D_{22}}}\boldsymbol{F}$ is known, and having calculated all the total forces ${}^{\mathbf{P_{32}}}\boldsymbol{F}^{*}$, ${}^{\mathbf{B_{52}}}\boldsymbol{F}^{*}$, ${}^{\mathbf{P_{22}}}\boldsymbol{F}^{*}$, ${}^{\mathbf{B_{32}}}\boldsymbol{F}^{*}$, ${}^{\mathbf{B_{42}}}\boldsymbol{F}^{*}$, ${}^{\mathbf{B_{12}}}\boldsymbol{F}^{*}$, ${}^{\mathbf{B_{31}}}\boldsymbol{F}^{*}$, ${}^{\mathbf{B_{41}}}\boldsymbol{F}^{*}$, ${}^{\mathbf{B_{11}}}\boldsymbol{F}^{*}$, all the forces acting on the linear hydraulic actuators can be found using the following expressions, going from the end-effector to the manipulator base:

$$ {}^{\mathbf{P_{32}}}\boldsymbol{F} = {}^{\mathbf{P_{32}}}\boldsymbol{F}^{*} + {}^{\mathbf{P_{32}}}\mathbf{U}_{\mathbf{D_{22}}}\, {}^{\mathbf{D_{22}}}\boldsymbol{F}, $$

$$ {}^{\mathbf{B_{52}}}\boldsymbol{F} = {}^{\mathbf{B_{52}}}\boldsymbol{F}^{*} + {}^{\mathbf{B_{52}}}\mathbf{U}_{\mathbf{P_{32}}}\, {}^{\mathbf{P_{32}}}\boldsymbol{F}, $$

$$ f_{c3} = \mathbf{x}_f^{T}\, {}^{\mathbf{B_{52}}}\boldsymbol{F}, $$

$$ {}^{\mathbf{P_{22}}}\boldsymbol{F} = {}^{\mathbf{P_{22}}}\boldsymbol{F}^{*} + {}^{\mathbf{P_{22}}}\mathbf{U}_{\mathbf{B_{52}}}\, {}^{\mathbf{B_{52}}}\boldsymbol{F}, $$

$$ {}^{\mathbf{P_{22}}}\boldsymbol{F} = {}^{\mathbf{P_{22}}}\boldsymbol{F}^{*} + {}^{\mathbf{P_{22}}}\mathbf{U}_{\mathbf{B_{52}}}\, {}^{\mathbf{B_{52}}}\boldsymbol{F}^{*} + {}^{\mathbf{P_{22}}}\mathbf{U}_{\mathbf{P_{32}}}\, {}^{\mathbf{P_{32}}}\boldsymbol{F}^{*} + {}^{\mathbf{P_{22}}}\mathbf{U}_{\mathbf{D_{22}}}\, {}^{\mathbf{D_{22}}}\boldsymbol{F}, $$

$$ f_{c2} = \mathbf{x}_f^{T}\, {}^{\mathbf{B_{42}}}\boldsymbol{F}^{*} - \frac{\mathbf{z}_\tau^{T}\left({}^{\mathbf{B_{12}}}\boldsymbol{F}^{*} + {}^{\mathbf{B_{12}}}\mathbf{U}_{\mathbf{P_{22}}}\, {}^{\mathbf{B_{12}}}\boldsymbol{F}\right)}{L_{21}\,\sin q_{22}} - \frac{\mathbf{z}_\tau^{T}\left({}^{\mathbf{B_{32}}}\boldsymbol{F}^{*}\right) + \mathbf{z}_\tau^{T}\left({}^{\mathbf{B_{42}}}\boldsymbol{F}^{*}\right) + \mathbf{y}_f^{T}\, {}^{\mathbf{B_{42}}}\boldsymbol{F}^{*}\,(x_2 + x_{20} - l_{c2})}{(x_2 + x_{20})\,\tan q_{22}}, $$

$$ {}^{\mathbf{B_{c2}}}\boldsymbol{F} = {}^{\mathbf{B_{c2}}}\boldsymbol{F}^{*} + {}^{\mathbf{B_{c2}}}\mathbf{U}_{\mathbf{B_{12}}}\, {}^{\mathbf{B_{12}}}\boldsymbol{F}^{*} + {}^{\mathbf{B_{c2}}}\mathbf{U}_{\mathbf{B_{32}}}\, {}^{\mathbf{B_{32}}}\boldsymbol{F}^{*} + {}^{\mathbf{B_{c2}}}\mathbf{U}_{\mathbf{B_{42}}}\, {}^{\mathbf{B_{42}}}\boldsymbol{F}^{*} + {}^{\mathbf{B_{c2}}}\mathbf{U}_{\mathbf{P_{22}}}\, {}^{\mathbf{P_{22}}}\boldsymbol{F}, $$

$$ f_{c1} = \mathbf{x}_f^{T}\, {}^{\mathbf{B_{41}}}\boldsymbol{F}^{*} - \frac{\mathbf{z}_\tau^{T}\left({}^{\mathbf{B_{11}}}\boldsymbol{F}^{*} + {}^{\mathbf{B_{11}}}\mathbf{U}_{\mathbf{B_{c2}}}\, {}^{\mathbf{B_{c2}}}\boldsymbol{F}\right)}{L_{11}\,\sin q_{12}} - \frac{\mathbf{z}_\tau^{T}\left({}^{\mathbf{B_{31}}}\boldsymbol{F}^{*}\right) + \mathbf{z}_\tau^{T}\left({}^{\mathbf{B_{41}}}\boldsymbol{F}^{*}\right) + \mathbf{y}_f^{T}\, {}^{\mathbf{B_{41}}}\boldsymbol{F}^{*}\,(x_1 + x_{10} - l_{c1})}{(x_1 + x_{10})\,\tan q_{12}}. $$

Additionally, forces/moments at any manipulator point can be calculated, as, for example:

$$ {}^{\mathbf{B_{c1}}}\boldsymbol{F} = {}^{\mathbf{B_{c1}}}\boldsymbol{F}^{*} + {}^{\mathbf{B_{c1}}}\mathbf{U}_{\mathbf{B_{11}}}\, {}^{\mathbf{B_{11}}}\boldsymbol{F}^{*} + {}^{\mathbf{B_{c1}}}\mathbf{U}_{\mathbf{B_{31}}}\, {}^{\mathbf{B_{31}}}\boldsymbol{F}^{*} + {}^{\mathbf{B_{c1}}}\mathbf{U}_{\mathbf{B_{41}}}\, {}^{\mathbf{B_{41}}}\boldsymbol{F}^{*} + {}^{\mathbf{B_{c1}}}\mathbf{U}_{\mathbf{B_{c2}}}\, {}^{\mathbf{B_{c2}}}\boldsymbol{F}. $$

In the attached simulation file, it is assumed that the manipulator is in the free-motion, thus ${}^{\mathbf{D_{22}}}\boldsymbol{F} = \mathbf{0}$.